14th International Conference on Structural Safety and Reliability - ICOSSAR'25
1-6 June, 2025 - Los Angeles California, USA
R. Ghanem, E. Johnson, S. Masri and A. Olivier (Eds)

SEISMIC FRAGILITY AND RISK ASSESSMENT OF MASONRY INFILLED LOW-DUCTILE RC FRAMES RETROFITTED WITH BRBS

RIFAN CHELAPRAMKANDY[1], JAYADIPTA GHOSH[2] AND FABIO FREDDI[3]

[1]Department of Civil Engineering, Indian Institute of Technology Bombay
Mumbai, India
rifanc@iitb.ac.in

[2]Department of Civil Engineering, Indian Institute of Technology Bombay
Mumbai, India
jghosh@iitb.ac.in and www.civil.iitb.ac.in/faculty/details/prof-jayadipta-ghosh

[3]Department of Civil, Environmental & Geomatic Engineering, University College London
London, UK
f.freddi@ucl.ac.uk and https://profiles.ucl.ac.uk/61999-fabio-freddi

Key words: Reinforced concrete frame, Unreinforced masonry infill, Buckling-restrained braces, Seismic retrofit, Seismic fragility, Seismic risk.

Abstract. *Masonry infilled reinforced concrete* (*RC*) *frames are a widely adopted construction typology worldwide, including areas with moderate to high seismicity. A large percentage of such structures were built before the implementation of modern seismic design codes, are vulnerable to seismic shaking, and need retrofitting. To this end, buckling-restrained braces* (*BRBs*) *have been proven to be an effective retrofit strategy for improving the seismic performance and safety of such structures. However, limited considerations have been made on the influence of masonry infills on the effectiveness of the retrofitting. Masonry infills are often overlooked in the seismic analysis and design of RC frames due to their brittle nature. However, recent research has shown that their strength and stiffness can significantly influence the seismic response of buildings structures, affecting seismic fragility and risk estimates. The present study investigates the impact of masonry infills on the seismic fragility and risk of low-ductile RC frames retrofitted with BRBs. A three-story, three-bay, low-ductile RC frame is selected for case study purposes. Finite element* (*FE*) *models for various structural configurations, i.e., Bare Frame, Infilled Frame, BRB-retrofitted Bare Frame, and BRB-retrofitted Infilled Frame, are developed in OpenSees. Nonlinear static and dynamic analyses are performed to evaluate the seismic performance of the case study structures. A cloud analysis-based approach, with a suite of ground motion records, is used to account for the record-to-record variability and develop seismic fragility curves. The study uses the average spectral acceleration as the intensity measure* (*IM*) *to account for the time period elongation resulting from the masonry infills and frame damage during seismic shaking. A seismic hazard curve is developed for the considered IM, and seismic risk estimates are derived. The results provide insights into the interaction between masonry infills and BRB retrofits, highlighting their impact on seismic fragility and risk.*

1 INTRODUCTION

Reinforced concrete (RC) frames with masonry infills are a common construction typology used worldwide, including regions with moderate to high seismic activity [1–3]. Existing RC frames designed before the introduction of modern seismic design codes are typically characterized by low ductility, often resulting in inadequate seismic performance [4–6]. Additionally, the complex interactions between masonry infills and the surrounding frames may increase the seismic vulnerability of these structures [3]. This underlines the urgent need to investigate the effectiveness of seismic retrofit strategies to address such structural deficiencies, while also accounting for the presence of masonry infills.

Supplemental damping devices are widely recognized as effective retrofit solutions for low-ductile frames [7]. These devices provide additional load paths and damping for the lateral loads induced by earthquake shaking, thereby reducing the seismic demand on the frame. Buckling-restrained braces (BRBs) are a kind of dissipative device capable of enhancing the strength, stiffness, and energy dissipation capacity of structures, thereby protecting them from earthquake-induced damage [8–11]. Unlike conventional braces, BRBs prevent buckling under compression loads by encasing a steel core within an unbonded restraining sleeve. This design allows the steel core to undergo large plastic deformations both in tension and compression, resulting in nearly symmetric hysteretic loops [12–14].

Masonry infills are often neglected in structural analysis and design due to their brittle behavior and classification as non-structural components. However, recent studies have shown that the stiffness and strength of the masonry infill may significantly influence the seismic performance of such structures. While masonry infills with a regular distribution may provide beneficial effects during seismic shaking [2], irregular distributions can lead to significant detrimental effects [15]. Moreover, the local interaction between the masonry infills and the surrounding frame can further magnify the seismic vulnerability of low-ductile RC frames [3]. Although numerous studies investigated the influence of masonry infills on RC frames, research on their impact on the effectiveness of retrofitting strategies remains minimal [16–18].

This study investigates the influence of masonry infills on the seismic fragility and risk of low-ductile RC frames retrofitted with BRBs. Finite element (FE) models of four case study structures are created using OpenSees [19], *i.e., Bare Frame*, *Infilled Frame*, *BRB-retrofitted Bare Frame*, and *BRB-retrofitted Infilled Frame*. Non-linear static analyses are conducted to estimate the seismic capacity of each structure. Subsequently, nonlinear time history analyses (NLTHAs) are performed to develop probabilistic seismic demand models (PSDMs) and seismic fragility curves. The study employs the average spectral acceleration (Sa_{avg}) as an intensity measure (*IM*) to account for the vibration period elongation related to masonry infills and RC frame damage during the seismic shaking. A seismic hazard curve is developed for the selected *IM*, and seismic risk estimates are derived through the convolution of seismic hazard with fragility. The results shed light on the influence of masonry infills on the effectiveness of the BRB retrofitting, highlighting their impact on seismic fragility and risk.

2 CASE STUDY DESCRIPTION AND FINITE ELEMENT MODELING

2.1 Description of case study RC frame

A three-story, three-bay, RC frame designed only for gravity loads is considered as a

representative case study in the paper. Extensive experimental work on a scaled model of the case study frame and its sub-assemblages have been conducted by previous researchers [20,21], facilitating a detailed FE model validation. The selected RC frame represents a common construction typology adopted in several regions of the US, European, and Asian countries [22,23] before the introduction of the modern seismic code. The frame was designed according to ACI 318-89 [24] without accounting for seismic loads. Due to the limited number of stories of the frames, wind loads were also neglected. As a result, the design process does not consider any lateral loads.

Figure 1 presents the layout of the case study structure, with uniformly distributed masonry infills, along with the BRB retrofit arrangement. The case study RC frame has a total height of 10.75 m, an interstory height of 3.66 m, and a bay width of 5.49 m. The beams have a rectangular cross-section with dimensions of 230 mm × 460 mm, while the columns have a square cross-section with dimensions of 300 mm × 300 mm. The concrete used in the RC frame has a compressive strength of 24 MPa, whereas the reinforcements are of Grade 40 steel with 276 MPa yield strength. Further details on the reinforcement layout of RC components and joints are available elsewhere in the literature [20,21].

The masonry infills considered in this study have square openings with a horizontal length equal to one-third of the panel length. These are made with a single line of bricks with a thickness of 92 mm. The material properties of the masonry infills are adopted from literature, with an elastic modulus of 1674.5 MPa, and a cracking strength of 0.18 MPa [25,26].

The BRBs are made by a series arrangement of an elastic brace and a BRB device. The properties of the BRBs have been defined according to Freddi *et al.* [9] as discussed in detail in the following sections.

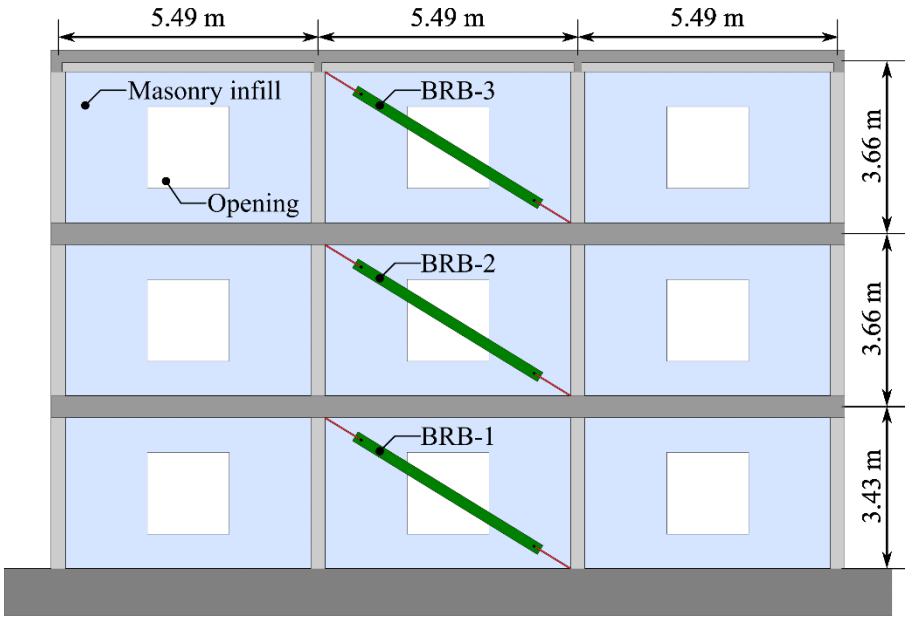

Figure 1: Layout of the case study RC frame with masonry infill and BRBs

FE models have been developed in OpenSees [19] for both the *Bare Frame* and *Infilled Frame*. Successively, BRBs are designed based on the structural response of the *Bare Frame*,

as conventionally done in practice. Incorporating BRBs into the FE models of the *Bare Frame* and *Infilled Frame*, provides the models of the *BRB-retrofitted Bare Frame* and *BRB-retrofitted Infilled Frame*, respectively.

2.2 Finite element (FE) modeling of RC frame

A two-dimensional FE model of the case study RC frame is developed in OpenSees [19]. Beams are modeled using *beamWithHinges* elements, while the *nonlinearBeamColumn* elements are used to model the columns. The concrete and reinforcement are modeled using the *Concrete02* and *Hysteretic* material models, respectively. According to the ACI 318-89 [24] recommendation, the effective slab width is taken as four times the beam width, and an unconfined concrete material model is used for modeling. The gravity loads are distributed on the beams, while the masses are concentrated at beam-column joints.

2.3 Finite element (FE) modeling of masonry infill

The presence of the masonry infills is accounted for through an equivalent double strut modeling approach, as shown in Figure 2A. This modeling strategy was preferred with respect to more widely used single strut models as it allows capturing the interaction between the masonry infills and the surrounding frames [27].

The backbone curve of the masonry infill is defined according to Dolšek and Fajfar [2]. Further details on the backbone definition and modeling approach can be found in Chelapramkandy *et al.* [18]. The resulting force-displacement backbone curve of the masonry infill is presented in Figure 2B.

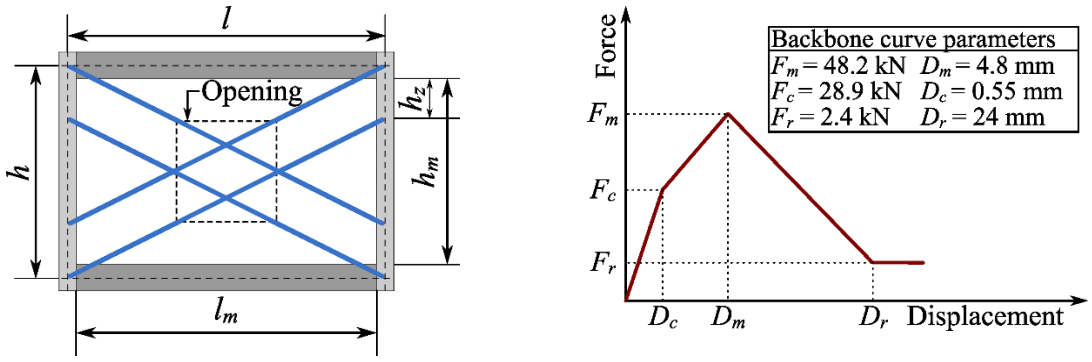

Figure 2: (A) Equivalent double strut modeling. (B) Backbone curve of masonry infill.

2.4 Design and finite element (FE) modeling of buckling-restrained braces (BRBs)

Conventionally, the BRBs' design does not account for the presence of the masonry infills, resulting in identical BRB design values for frames with and without infills. The main objectives of BRB design are briefly outlined below, with a more comprehensive discussion available in the relevant literature [8,9,18,28,29]. The dimensions of the BRBs are designed to achieve the target base shear capacity for the retrofitted structure. The distribution of the stiffness, strength, and ductility among the stories is designed such that 1) they do not alter the fundamental mode shape of the bare frame, 2) all BRBs yield together, and 3) all BRBs reach their maximum ductility capacity at the design displacement.

The BRBs consist of an elastic brace and a BRB device arranged in series. BRB devices are modeled using the *steelBRB* material model, while the elastic braces are modeled through a truss element. Additional details are available in Chelapramkandy *et al.* [18]. The design values of the BRBs are presented in Table 1. In this table, K_d and F_d represent the stiffness and strength of the dissipative braces in each story. The properties of the BRB device (A_{BRB} - cross-sectional area, L_{BRB} - length, F_{BRB} - strength, and K_{BRB} - stiffness) and elastic braces (A_{eb} - cross-sectional area, L_{eb} - length, F_{eb} - strength, and K_{eb} - stiffness) are also listed.

Table 1: Design parameters of BRBs

Story	Dissipative braces		BRB devices				Elastic braces			
	F_d [kN]	K_d [kN/mm]	A_{BRB} [mm^2]	L_{BRB} [mm]	F_{BRB} [kN]	K_{BRB} [kN/mm]	A_{eb} [mm^2]	L_{eb} [mm]	F_{eb} [kN]	K_{eb} [kN/mm]
1	218.9	54.2	875.7	2499.9	218.9	73.6	3501.6	3569.9	1183.9	206.0
2	190.3	33.8	761.0	3487.2	190.3	45.8	1653.9	2706.6	559.2	128.3
3	110.7	29.5	442.7	2321.5	110.7	40.0	2067.8	3872.3	699.1	112.1

3 SEISMIC FRAGILITY ASSESSMENT

This section outlines the process for developing fragility curves for all case study structures. Initially, the seismic capacity of the case study structures is estimated through pushover analyses. Successively, PSDMs and fragility curves are derived based on the response obtained from NLTHAs.

3.1 Pushover analysis and damage state (DS) thresholds estimation

The engineering demand parameter (*EDP*) adopted in the present study is the maximum interstory drift ratio (IDR_{max}). The pushover analysis is conducted on all case study structures *i.e., Bare Frame, Infilled Frame, BRB-retrofitted Bare Frame,* and *BRB-retrofitted Infilled Frame*. Figure 3A shows the base shear *vs*. IDR_{max} curve for the different case-study structures. The damage state (DS) of the structural components is categorized as Slight, Moderate, Extensive, and Complete, determined by the exceedance of threshold values of local *EDP* of the structural component, as detailed in Table 2.

The *Bare Frame* exhibits a gradual increase of the base shear and attains a peak value of 196.95 kN. The *Infilled Frame* shows a sharp increase in base shear due to the additional stiffness and strength of the masonry infill. After reaching the peak, the base shear decreases, which is associated with the softening of the masonry infill panel. Due to the unsymmetric placement of the BRBs, pushover analyses are performed in both directions (rightward: +ve and leftward: -ve), resulting in a minor difference in the base shear *vs*. IDR_{max} plot and the corresponding DS threshold values. The DS thresholds for the frame with BRBs are taken as the average of the results from the pushover performed in both directions.

The difference in the DS threshold values for Slight and Complete DSs among all frames is minimal. Conversely, the DS Moderate threshold values show a significant difference. This is due to the damage of the masonry infill and the subsequent redistribution of the axial and shear forces from the infill panel to the surrounding frame, resulting in the concrete strain increasing

suddenly. As a result, the onset of Moderate DS of the infilled frames occurs at a lower IDR_{max}. The DS threshold values for the Extensive DS are provided by the average of the Moderate and Complete and are at intermediate values. For further details, the reader can refer to Chelapramkandy *et al.* [18].

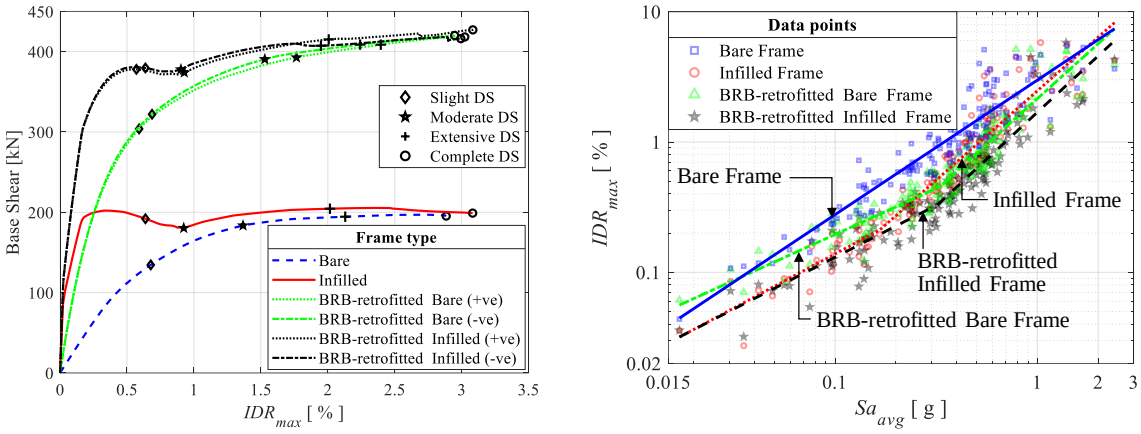

Figure 3: (A) Base shear *vs.* IDR_{max} plot; (B) PSDM of case study structures.

Table 2: DS definition and threshold values.

Damage States	**Description**	**DS threshold values**			
		Bare Frame	Infilled Frame	BRB-retrofitted Bare Frame	BRB-retrofitted Infilled Frame
	Building frame	IDR_{max} [%]			
Slight	Yielding of rebars in 50% columns in a story	0.68	0.64	0.64	0.60
Moderate	Concrete crushing/spalling in 50% columns in a story	1.37	0.92	1.65	0.92
Extensive	Average of Moderate and Complete	2.13	2.02	2.32	1.98
Complete	Shear failure initiation in 50% of columns in a story	2.88	3.08	2.99	3.04

3.2 Probabilistic Seismic Demand Models (PSDMs)

The configurations accounting for the presence of the masonry infills are characterized by significant period elongation due to the early damage and softening of the infills. Therefore, the present study uses the average spectral acceleration (Sa_{avg}) as the intensity measure (*IM*). The boundary periods of the Sa_{avg} are defined explicitly accounting for the period elongation in such structures. Sa_{avg} for a specified period band can be defined as follows [30]:

$$Sa_{avg}\left(T_1,T_2,...T_n\right)=\left(\prod_{i=1}^{n}Sa\left(T_i\right)\right)^{1/n} \quad (1)$$

where Sa(T_i) is the spectral acceleration at the i^{th} time period (T_i). The present study adopts the lower limit of the period band corresponding to the fundamental period of the stiffest structure,

i.e., BRB-retrofitted Infilled Frame at its intact state. The upper limit is assumed as the average of the fundamental period of the *Bare Frame* after it has undergone seismic damage. The resulting period band for this study ranges from 0.22 s to 1.25 s.

A cloud analysis-based approach with a suite of 150 ground motions [31] is utilized to develop PSDMs. The results of the NLTHAs, *i.e.*, the *EDP-IM* pairs – specifically the IDR_{max}-Sa_{avg} pairs, are used to derive the PSDMs in a log-log space [32]. While a linear PSDM is developed for the *Bare Frame*, bilinear PSDMs were found to be a more suitable choice for the structure with masonry infills and BRB retrofits [33–35]. The expressions for the linear and bilinear PSDM are as follows:

$$\ln(EDP) = a + b \times \ln(IM) + \varepsilon \tag{2}$$

$$\ln(EDP) = \left[a_1 + b_1 \times \ln(IM)\right] H_1 + \left[a_2 + b_2 \times \ln(IM)\right](1 - H_1) + \varepsilon \tag{3}$$

where a, b, a_1, b_1, a_2, b_2 are the regression coefficients; $H_1 = 0$, when $IM > IM^*$ and $H_1 = 1$ otherwise. The value of IM^* corresponds to *IM* at the intersection of two branches of bilinear PSDM and is chosen such that the bilinear PSDM gives better goodness-of-fit [33]; ε is a normal random variable representing regression error with zero mean. The PSDMs for various case study structures are presented in Figure 3B and the associated regression parameters and goodness-of-fit estimates are listed in Table 3.

Table 3: Parameters associated with PSDMs

Building type	a_1 **(or** a**)**	b_1 **(or** b**)**	$\beta_{EDP\|IM1}$	a_2	b_2	$\beta_{EDP\|IM2}$	IM^*	R^2
Bare Frame	-3.51	1.03	0.34	-	-	-	-	0.87
Infilled Frame	-4.67	0.83	0.27	-3.70	1.37	0.35	0.17	0.91
BRB-retrofitted Bare Frame	-4.62	0.70	0.24	-3.84	1.40	0.35	0.33	0.89
BRB-retrofitted Infilled Frame	-4.81	0.80	0.31	-4.08	1.44	0.32	0.32	0.90

The seismic demand based on the IDR_{max} is lower for the *Infilled Frame* compared to the *Bare Frame* at the lower seismic intensities, as shown in Figure 3B. This difference diminishes as the intensity increases. The observed behavior is because the influence of the masonry infills is significant at the lower intensities and diminished at the higher intensities due to the seismic damage. A similar trend is observed for the retrofitted cases. The *BRB-retrofitted Infilled Frame* exhibits a significant difference compared to the *BRB-retrofitted Bare Frame* at lower intensities, with the difference diminishing as the intensity increases.

3.3 Seismic Fragility

The seismic fragility is determined based on the seismic capacity and seismic demand models for the case study structures. Seismic fragility refers to the probability of exceeding a DS given an *IM* [36], and it is expressed as follows:

$$P[DS \mid IM] = \Phi\left[\frac{\ln(EDP_{med} / S_C)}{\sqrt{\beta_{EDP|IM}^2 + \beta_C^2}}\right]; \text{ where, } \beta_{EDP|IM} \cong \sqrt{\frac{\sum\left\{\ln(EDP) - \left[a + b \times \ln(IM)\right]\right\}^2}{N - 2}} \tag{4}$$

In the above equation, EDP_{med} and $\beta_{EDP|IM}$ represent, respectively, the median and dispersion of an *EDP*, where *N* is the number of *EDP* samples. Additionally, S_C and β_C are the seismic capacity estimates and their corresponding dispersion. The seismic capacity is assumed

to follow a lognormal distribution with a dispersion of 0.3 [37]. For bilinear demand models, the PSDM for both branches is utilized to estimate seismic fragility by applying the maximum likelihood estimation method to fit the lognormal distribution [38]. The resulting seismic fragility curve parameters in terms of median (med.) and dispersion (disp.) for the case study structures are provided in Table 4, while some of the fragility curves are shown in Figure 4.

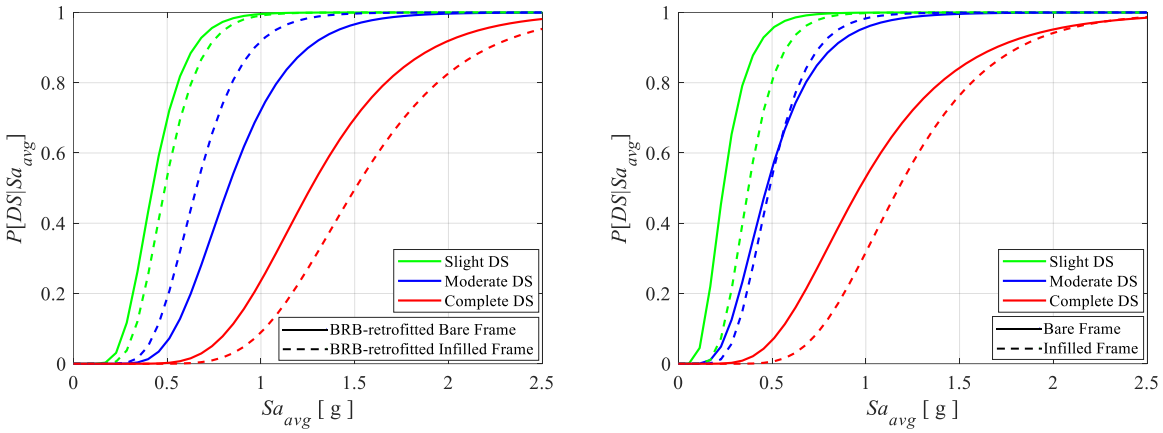

Figure 4: Comparison of seismic fragility curves between (A) BRB-retrofitted frames and (B) unretrofitted frames.

In general, the seismic fragility of the *BRB-retrofitted Infilled frame* is lower than that of the *BRB-retrofitted Bare frame* across all DS, except for the Moderate DS, as shown in Figure 4A and detailed in Table 4. The increased fragility at the Moderate DS is due to the seismic capacity of the *BRB-retrofitted Infilled Frame* being significantly lower than that of the *BRB-retrofitted Bare frame*. Similarly, the seismic fragility of the *Infilled frame* is lower than that of the *Bare frame* for all DS, with the exception of the Moderate DS, where the reduction is negligible, as shown in Figure 4B. This discrepancy is attributed to the significantly lower seismic capacity of the *Infilled Frame* relative to the *Bare Frame* for Moderate DS.

Table 4: Parameters associated with seismic fragilities

	Slight		**Moderate**		**Extensive**		**Complete**	
Building type	**med.**	**disp.**	**med.**	**disp.**	**med.**	**disp.**	**med.**	**disp.**
Bare frame	0.239	0.438	0.470	0.438	0.721	0.438	0.966	0.438
Infilled frame	0.373	0.339	0.486	0.339	0.864	0.339	1.175	0.339
BRB-retrofitted Bare Frame	0.421	0.327	0.824	0.327	1.056	0.327	1.265	0.327
BRB-retrofitted Infilled Frame	0.487	0.303	0.655	0.303	1.116	0.303	1.504	0.303

4 SEISMIC RISK ASSESSMENT

This section focuses on the seismic risk assessment of the case study structures. Initially, the seismic hazard curve is derived for a case study site using Sa_{avg} as *IM*. Subsequently, the hazard curve is convolved with the seismic fragility to provide seismic risk estimates, which are then compared across the case study structures.

4.1 Seismic Hazard Analysis

The present study develops a hazard curve for Sa_{avg} considering a hypothetical site [39]. Probabilistic Seismic Hazard Analysis is performed following the methodology outlined by Baker [39]. The ground motion prediction equation proposed by Boore and Atkinson [40] is used. The expression provided by Baker and Jayaram [30] was used to develop the correlation coefficients of spectral acceleration. Figure 5A shows the resulting seismic hazard curve.

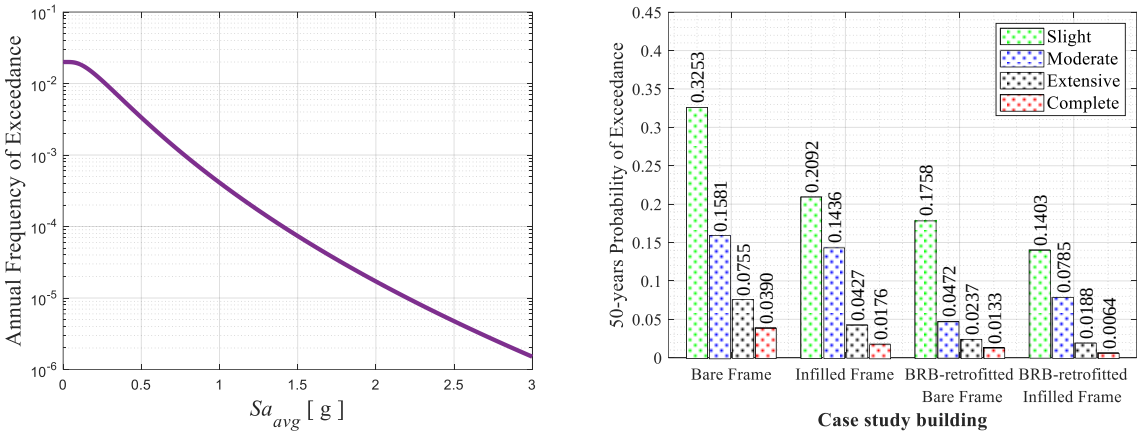

Figure 5: (A) Seismic hazard curve. (B) Seismic risk estimates

The seismic risk of a building structure is estimated by convoluting its seismic fragility with the seismic hazard [$H(IM = im)$]. The 50-year (T = 50) risk is calculated as follows [41]:

$$P_{Tf} = 1-(1-P_{Af})^{T} \tag{5}$$

where P_{Af} represents the annual probability of the exceedance expressed as follows [41]:

$$P_{Af} = \int_{im} [Fragility \mid IM = im] \left| \frac{dH(im)}{d(im)} \right| d(im) \tag{6}$$

Seismic risk is estimated for various DSs across the different configurations of the case study structure, as shown in Figure 5B. The seismic risk follows a trend similar to that of the seismic fragility since the hazard curve is consistent across all the case study structures. As compared to the *BRB-retrofitted Bare Frame*, the *BRB-retrofitted Infilled Frame* exhibits a 21%, 21%, and 52%, reduction in seismic risk for the Slight, Extensive, and Complete DS, respectively. However, for Moderate DS, the seismic risk increased by 66%, as shown in Figure 5B. Similarly, the *Infilled Frame* exhibits a 36%, 9%, 44%, and 55% reduction in seismic risk corresponding to Slight, Moderate, Extensive, and Complete DS, respectively, as compared to the *Bare Frame*. It can observed that for Moderate DS, the reduction in seismic risk is less than other DS, similar to the pattern observed in the seismic fragility estimates.

5 CONCLUSIONS

This paper examines the influence of unreinforced masonry infill on the seismic fragility and risk estimates of infilled reinforced concrete (RC) frames retrofitted with buckling-restrained braces (BRBs). A three-story, three-bay, low-ductile RC frame is selected for case study purposes. Finite element (FE) models for various structural configurations, *i.e.*, *Bare Frame*,

Infilled Frame, *BRB-retrofitted Bare Frame*, and *BRB-retrofitted Infilled Frame*, are developed in OpenSees. Nonlinear static and dynamic analyses are performed to evaluate the seismic performance of the case study structures. A cloud analysis-based approach, with a suite of ground motion records, is used to account for the record-to-record variability and develop seismic fragility curves for different damage states (DSs). The study uses the average spectral acceleration as the intensity measure (*IM*) to account for the vibration period elongation resulting from the masonry infills and frame damage during seismic shaking. A seismic hazard curve is developed for the considered *IM*, and seismic risk estimates are derived. The key conclusions drawn from the present study are as follows:

- The presence of the masonry infill reduces the seismic capacity of the frame at the Moderate DS when compared to the frame without masonry infills.
- The influence of the masonry infills is significant at a lower intensity and diminishes as intensity increases.
- In general, the seismic fragility and associated risk of *the BRB-retrofitted Infilled Frame* is lower than that of the *BRB-retrofitted Bare frame* across all DS, except for Moderate DS.

This finding underscores the importance of considering the presence of masonry infills during the seismic analysis and design stage. Future work will include the influence of the masonry infills on the seismic life-cycle estimation and the effects of non-uniformly distributed masonry infills on the seismic performance of the low-ductile RC frames.

REFERENCES

[1] Sattar, S. Liel, A.B. Seismic performance of nonductile reinforced concrete frames with masonry infill walls - I: Development of a strut model enhanced by finite element models. *Earthq Spectra* (2016) **32**:795–818.

[2] Dolšek, M. Fajfar, P. The effect of masonry infills on the seismic response of a four-storey reinforced concrete frame - a deterministic assessment. *Eng Struct* (2008) **30**:1991–2001.

[3] Di Trapani, F. Macaluso, G. Cavaleri, L. Papia, M. Masonry infills and RC frames interaction: Literature overview and state of the art of macromodeling approach. *Eur J Environ Civ Eng* (2015) **19**:1059–1095.

[4] Freddi, F. Novelli, V. Gentile, R. *et al.* Observations from the 26th November 2019 Albania earthquake: the earthquake engineering field investigation team (EEFIT) mission. *Bull Earthq Eng* (2021) **19**:2013–2044.

[5] Rao, A. Dutta, D. Kalita, P. *et al.* Probabilistic seismic risk assessment of India. *Earthq Spectra* (2020) **36**:345–371.

[6] Rossetto, T. Elnashai, A. Derivation of vulnerability functions for European-type RC structures based on observational data. *Eng Struct* (2003) **25**:1241–1263.

[7] Soong, T.T. Spencer, B.F. Supplemental energy dissipation: State-of-the-art and state-of-the-practice. *Eng Struct* (2002) **24**:243–259.

[8] Freddi, F. Tubaldi, E. Ragni, L. Dall'Asta, A. Probabilistic performance assessment of low-ductility reinforced concrete frames retrofitted with dissipative braces. *Earthq Eng Struct Dyn* (2013) **42**:993–1011.

[9] Freddi, F. Ghosh, J. Kotoky, N. Raghunandan, M. Device uncertainty propagation in low-ductility RC frames retrofitted with BRBs for seismic risk mitigation. *Earthq Eng Struct*

Dyn (2021) **50**:2488–2509.
[10] Gutiérrez-Urzúa, F. Freddi, F. Tubaldi, E. Seismic risk and failure modes assessment of steel BRB frames under earthquake sequences. *Struct Saf* (2025) **115**: 102598.
[11] Freddi, F. Wu, J.R. Cicia, M. *et al.* Seismic Retrofitting of Existing Steel Frames with External BRBs: Pseudo-Dynamic Hybrid Testing and Numerical Parametric Analysis. *Earthq Eng Struct Dyn* (2025) **54**:1064–1083.
[12] Zona, A. Dall'Asta, A. Elastoplastic model for steel buckling-restrained braces. *J Constr Steel Res* (2012) **68**:118–125.
[13] Black, C.J. Makris, N. Aiken, I.D. Component Testing, Seismic Evaluation and Characterization of Buckling-Restrained Braces. *J Struct Eng* (2004) **130**:880–894.
[14] Tremblay, R. Bolduc, P. Neville, R. DeVall, R. Seismic testing and performance of buckling-restrained bracing systems. *Can J Civ Eng* (2006) **33**:183–198.
[15] Negro, P. Colombo, A. Irregularities induced by nonstructural masonry panels in framed buildings. *Eng Struct* (1997) **19**:576–585.
[16] Castaldo, P. Tubaldi, E. Selvi, F. Gioiella, L. Seismic performance of an existing RC structure retrofitted with buckling restrained braces. *J Build Eng* (2021) **33**:101688.
[17] Ruiz, S.E. Santos-Santiago, M.A. Bojórquez, E. *et al.* BRB retrofit of mid-rise soft-first-story RC moment-frame buildings with masonry infill in upper stories. *J Build Eng* (2021) **38**.
[18] Chelapramkandy, R. Ghosh, J. Freddi, F. Influence of masonry infills on seismic performance of BRB-retrofitted low-ductile RC frames. *Earthq Eng Struct Dyn* (2025) **54**:295–318.
[19] McKenna, F. Fenves, G. Scott, M. Open system for earthquake engineering simulation. *Pacific Earthq Eng Res Cent* (2000).
[20] Aycardi, L.E. Mander, J.B. Reinhorn, A.M. Seismic resistance of reinforced concrete frame structures designed only for gravity loads: Experimental performance of subassemblages. *ACI Mater J* (1994) **91**:552–563.
[21] Bracci, J.M. Reinhorn, A.M. Mander, J.B. Seismic resistance of reinforced concrete frame structures designed for gravity loads: performance of structural system. *ACI Mater J* (1995) **92**:597–609.
[22] Lang, D.H. Kumar, A. Sulaymanov, S. Meslem, A. Building typology classification and earthquake vulnerability scale of Central and South Asian building stock. *J Build Eng* (2018) **15**:261–277.
[23] Crowley, H. Despotaki, V. Silva, V. *et al.* Model of seismic design lateral force levels for the existing reinforced concrete European building stock. *Bull Earthq Eng* (2021) **19**:2839–2865.
[24] ACI Committee 318. *Building Code Requirements for Reinforced Concrete and Commentary (ACI 318-89/ACI 318R-89)*. American Concrete Institute; 1989.
[25] Cobanoglu, B. Aldemir, A. Demirel, İ.O. Binici, B. Canbay, E. Yakut, A. Seismic Performance Assessment of Masonry Buildings Using In Situ Material Properties. *J Perform Constr Facil* (2017) **31**:1–12.
[26] Allen, M.H. Taylor, R.B. *Compressive, Transverse and Racking Strength of four-inch brick walls*. Structural Clay Products Research Foundation, Geneva, Illinois; 1965.
[27] Wu, J.R. Di Sarno, L. Freddi, F. D'Aniello, M. Modelling of masonry infills in existing steel moment-resisting frames: Nonlinear force-displacement relationship. *Eng Struct*

(2022) **267**:114699.
[28] Ragni, L. Zona, A. Dall'Asta, A. Analytical expressions for preliminary design of dissipative bracing systems in steel frames. *J Constr Steel Res* (2011) **67**:102–113.
[29] Gutiérrez-Urzúa, F. Freddi, F. Influence of the design objectives on the seismic performance of steel moment resisting frames retrofitted with buckling restrained braces. *Earthq Eng Struct Dyn* (2022) **51**:3131–3153.
[30] Baker, J.W. Jayaram, N. Correlation of spectral acceleration values from NGA ground motion models. *Earthq Spectra* (2008) **24**:299–317.
[31] Smerzini, C. Galasso, C. Iervolino, I. Paolucci, R. Ground motion record selection based on broadband spectral compatibility. *Earthq Spectra* (2014) **30**:1427–1448.
[32] Cornell, C.A. Jalayer, F. Hamburger, R.O. Foutch, D.A. Probabilistic Basis for 2000 SAC Federal Emergency Management Agency Steel Moment Frame Guidelines. *J Struct Eng* (2002) **128**:526–533.
[33] Tubaldi, E. Freddi, F. Barbato, M. Probabilistic seismic demand model for pounding risk assessment. *Earthq Eng Struct Dyn* (2016) **45**:1743–1758.
[34] Freddi, F. Padgett, J.E. Dall'Asta, A. Probabilistic seismic demand modeling of local level response parameters of an RC frame. *Bull Earthq Eng* (2017) **15**:1–23.
[35] O'Reilly, G.J. Monteiro, R. Probabilistic models for structures with bilinear demand-intensity relationships. *Earthq Eng Struct Dyn* (2019) **48**:253–268.
[36] Porter, K. Kennedy, R. Bachman, R. Creating fragility functions for performance-based earthquake engineering. *Earthq Spectra* (2007) **23**:471–489.
[37] HAZUS-MH MR4. *Technical Manual - Multi-hazard Loss Estimation Methodology, Earthquake Model*. Washington, DC: Federal Emergency Management Agency; 2003.
[38] Baker, J.W. Efficient analytical fragility function fitting using dynamic structural analysis. *Earthq Spectra* (2015) **31**:579–599.
[39] Baker, J.W. An introduction to Probabilistic Seismic Hazard Analysis (PSHA). *Bak Res Gr* (2008):1–72.
[40] Boore, D.M. Atkinson, G.M. Ground-motion prediction equations for the average horizontal component of PGA, PGV, and 5%-damped PSA at spectral periods between 0.01 s and 10.0 s. *Earthq Spectra* (2008) **24**:99–138.
[41] Padgett, J.E. Dennemann, K. Ghosh, J. Risk-based seismic life-cycle cost-benefit (LCC-B) analysis for bridge retrofit assessment. *Struct Saf* (2010) **32**:165–173.